# NIH RELAIS Document Delivery

NIH-10286730

JEFFDUYN

NIH -- W1 MA34IF

JOZEF DUYN
10 Center Dirve
Bldg. 10/Rm.1L07
Bethesda, MD 20892-1150

ATTN:
PHONE: 301-594-7305
FAX: -
E-MAIL:

SUBMITTED: 2002-08-29 17:22:17
PRINTED: 2002-09-03 07:32:46
REQUEST NO.:NIH-10286730
SENT VIA: LOAN DOC
7967415

---

NIH Fiche to Paper Journal

---

TITLE: MAGNETIC RESONANCE IN MEDICINE : OFFICIAL JOURNAL OF THE SOCIETY OF MAGNETIC RESONANCE IN MEDICINE / SOCIETY OF MAGNETIC RESONANCE IN MEDICINE
PUBLISHER/PLACE: Wiley-Liss, Inc., a division of John Wil New York, NY :
VOLUME/ISSUE/PAGES:1996 Mar;35(3):356-63 356-63
DATE: 1996
AUTHOR OF ARTICLE: Soher BJ; van Zijl PC; Duyn JH; Barker PB
TITLE OF ARTICLE: Quantitative proton MR spectroscopic imaging of th
ISSN: 0740-3194
OTHER NOS/LETTERS: Library reports holding volume or year
8505245
8699947
SOURCE: PubMed
CALL NUMBER: W1 MA34IF
REQUESTER INFO: JEFFDUYN
DELIVERY: E-mail: jhd@helix.nih.gov
REPLY: Mail:

# Quantitative Proton MR Spectroscopic Imaging of the Human Brain

Brian J. Soher, Peter C.M. van Zijl, Jeffrey H. Duyn, Peter B. Barker

**Multislice proton MR spectroscopic images (SI) of the brain were quantitated, using the phantom replacement technique. In 16 normal volunteers, ranging in age from 5 to 74 years, average "whole brain" concentrations of choline (Cho), creatine (Cr), and *N*-acetylaspartate (NAA) were found to be 2.4 ± 0.4, 7.9 ± 1.3, and 11.8 ± 1.0 (m*M*, mean ± SD), respectively. These values are in good general agreement with those previously determined by single-voxel localization techniques. Cortical gray matter was found to have lower Cho and NAA levels, compared to those of white matter, corpus callosum, and basal ganglia. Cho was also found to increase significantly with age in several locations. Quantitative multislice proton SI is feasible in the clinical environment, and regional and age-dependent variations occur that must be accounted for when evaluating spectra from pathological conditions.**

**Key words: proton MR spectroscopy; quantitation.**

## INTRODUCTION

Quantitation remains an important issue in clinical proton spectroscopy of the human brain. The common practice of measuring metabolite ratios, although in some cases providing a sensitive index of pathological changes (for instance, when two metabolites change in opposite directions), may be misleading or even be normal if parallel changes occur in all metabolite levels simultaneously. Similarly, comparisons to contralateral brain regions (which are assumed to be metabolically normal) may not be possible in many cases in which patients have either bilateral or global metabolic defects. Therefore, it is important to develop a simple and robust absolute quantitation scheme for clinical spectroscopy. In addition, normal variations in metabolite concentration must be known before the significance of pathological change can be assessed.

Metabolite levels and peak assignments in proton brain spectra have been studied extensively, using single-voxel spatial localization techniques, and there is now a general consensus concerning peak assignments and metabolite concentrations of the major resonances in the *in vivo* proton spectrum (1–8). However, single-voxel localization techniques have a number of limitations in the context of clinical spectroscopy; voxel sizes are often relatively large, and no information is available concerning spatial distribution or extent of metabolic abnormalities. In contrast, spectroscopic imaging (SI) (9–12) has significant advantages in terms of spatial resolution, efficiency of data collection, and mapping the distribution of cerebral metabolite levels. Despite these advantages, there have been few reports of quantitative proton SI of the human brain (13, 14), mainly because many of the quantitation techniques used in single-voxel localization methods are difficult to adapt to SI. For instance, it may take a prohibitively long time to record a water SI data set for use as an internal reference (3), and external standards may lie beyond the region excited by the pulse sequence (e.g., STEAM or PRESS (15)), or in the region affected by outer volume saturation pulses, which may be used for lipid suppression (11).

This article presents the quantitative results of a multislice spectroscopic imaging study, using an adaptation of the phantom replacement method (7, 16). This method has the advantage that no additional patient scan time is required above the normal clinical SI examination, and it can be used in conjunction with any spatial localization pulse sequence. Ten representative regions were chosen for quantitative analysis, and metabolite levels were examined for correlations with patient age and spatial location.

## METHODS

### Volunteer Population and MR Techniques

Eleven male and five female volunteers (age range 5–74 years, 39 ± 20 years (mean ± SD)), free of any known neuropathological condition, were studied in a standard GE 1.5-Tesla MR scanner (General Electric Medical Systems, Milwaukee, WI), using a combined MR and spectroscopic imaging protocol. All studies used the standard GE quadrature birdcage head coil. MRI consisted of a routine brain examination, namely, sagittal $T_1$-weighted images (5 mm thick, $TR$ = 625 ms, $TE$ = 20 ms) and oblique axial double-echo spin density and $T_2$-weighted (5 mm thick, $TR$ = 3000 ms, $TE$ = 31 and 100 ms). Spectroscopic imaging was performed, using a multislice spin-echo sequence with outer volume suppression (11). Four oblique slices were recorded with a 15 mm thickness and a gap of 2.5 mm. The $TR$ was 2300 ms and $TE$ 272 ms. A 32 × 32 circular phase-encoding scheme resulted in a total data acquisition time of 30 min (1 "NEX"). The field of view was 24 cm, giving a nominal voxel size of 15 × 8 × 8 mm (≈ 0.8 cm$^3$). The full echo signal was digitized with 256 data points and a spectral width of 1000 Hz. Water suppression was accomplished with a single chemical shift selective pulse (17, 18) with a bandwidth of 110 Hz. Extracranial lipid signals were attenuated by the use of eight outer volume saturation

**MRM 35:356–363 (1996)**

From the Russell H. Morgan Department of Radiology and Radiological Science (B.J.S., P.C.M.V.Z., P.B.B.), Johns Hopkins University School of Medicine, Baltimore, Maryland; and Laboratory of Diagnostic Radiology Research (J.H.D.), National Institutes of Health, Bethesda, Maryland.

Address correspondence to: Peter B. Barker, Ph.D., Department of Neurology, Henry Ford Hospital, 2799 W. Grand Boulevard, Detroit, MI 48202.

Received June 30, 1995; revised September 26, 1995; accepted September 26, 1995.This work was supported in part by the Whitaker Foundation, Washington, DC, and by NIH Grants NS 31490 and NS 32833.

0740-3194/96 $3.00

pulses, arranged in an octagonal pattern in an attempt to match the contours of the skull. $T_1$-weighted MR images (15 mm thick, $TR$ = 400 ms, $TE$ = 20 ms) were recorded at the same slice locations as the SI data set for anatomical correlation. A final set of double-gradient-echo images (45° flip angle, $TR$ = 250 ms, $TE$ = 10 and 20 ms, 1 NEX, 128 × 256) were also recorded at the same slice locations to calculate maps of the $B_0$ magnetic field strength. The complete examination lasted for 1 h.

All oblique MR and SIs were performed in a plane parallel to the anterior commissure-posterior commissure line, identified from the midline sagittal localizer image. The four SI slices were chosen so that the most caudal slice was at the level of the third ventricle, slightly above the tentorium; usually, the second slice included the lateral ventricles, the third slice occurred at the centrum semiovale, and the top slice contained mainly cortical gray matter (Fig. 1A).

A 4.6-liter phantom consisting of 20 m*M* creatine (Cr), 0.6% sodium chloride, and lightly doped with nickel chloride was studied, using the same SI methodology, for quantitation purposes. Phantom relaxation time measurements ($T_1/T_2$) were made by varying $TR$ and $TE$ and fitting the resulting data to the equation

$$S = S_0 * \exp(-TE/T_2) * (1 - \exp(-TR/T_1)) \quad [1]$$

*In vivo* metabolite relaxation times were taken from a previous study of 10 normal volunteers (3), and the following values were used: Cho: $T_1$ = 1.2 s, $T_2$ = 0.36 s; Cr: $T_1$ = 1.6 s, $T_2$ = 0.21 s; NAA: $T_1$ = 1.5 s, $T_2$ = 0.43 s.

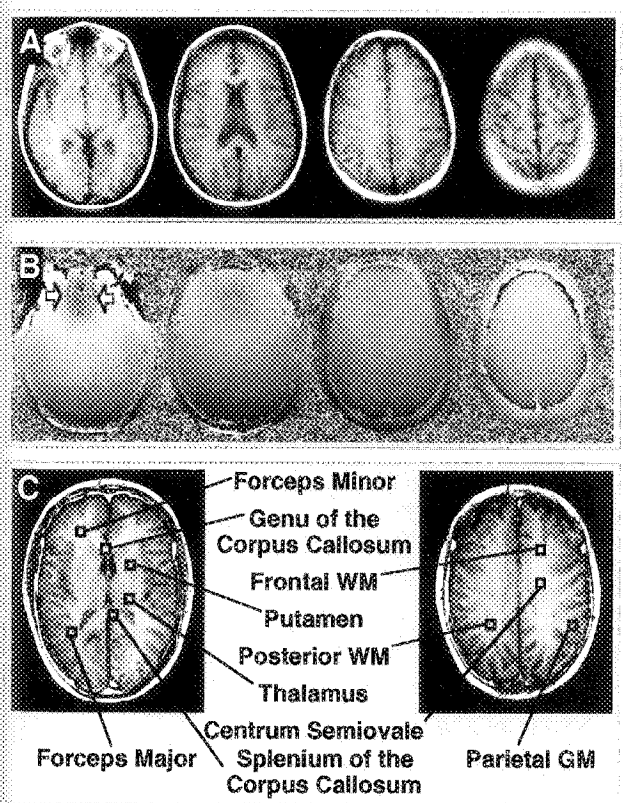


FIG. 1. (A) $T_1$-weighted localizer images, showing slice locations of spectroscopic images, and (B) $B_0$ field maps reconstructed from the double-echo gradient-echo sequence. The gray scale corresponds to a frequency range of -50 Hz (black) to +50 Hz (white). Note poor field homogeneity in the anterior region of the most caudal slice (arrows), due to the magnetic susceptibility effect of the air-tissue interface of the sphenoid sinus. (C) Regions of interest chosen for quantitative spectral analysis. WM, white matter; GM, gray matter.

### Quantitation Methodology and Data Analysis

Spectroscopic images of choline (Cho), Cr, and NAA were reconstructed, using 3-dimensional Fourier transformation. Before Fourier transformation, a cosine filter was applied in the spatial dimensions, and an exponential line broadening of 3 Hz, zero-filling to 2048 data points, and a high-pass convolution filter to remove the residual water signal (50-Hz stop band (19)) were applied in the time domain. A frequency correction was also applied, based on the field maps calculated from the gradient-echo scans. Metabolite images were calculated by integration of magnitude peak areas (integration range 0.2 ppm), followed by linear interpolation from the original 32 × 32 matrix size to 256 × 256 points. No base-line correction was needed, because the long-echo-time spin-echo spectra have very flat baselines.

Ten brain regions were chosen for quantitative analysis, namely, forceps major, thalamus, the splenium and genu of the corpus callosum, putamen, forceps minor, frontal lobe white matter, centrum semiovale, posterior white matter, and frontoparietal gray matter (Fig. 1C). Inasmuch as it has recently been shown that no left-right asymmetries occur in metabolite levels in normal human brain, voxels were chosen arbitrarily on the left or right (20), depending on which side gave a better registration between the spectroscopic region of interest (SI grid) and the anatomical structure under investigation. Magnitude spectra from each of these regions (and the phantom) were analyzed in the frequency domain, using a Nelder-Mead simplex algorithm ("Numerical Recipes," (21)). The experimental data were assumed to be of the form

$$f(\omega) = \sum_{i=1}^{N} A(\omega - \omega_i) \otimes \mathrm{sinc}((\omega - \omega_i)/P) \quad [2]$$

where $A(\omega)$ is the Lorentzian "absorption" lineshape

$$A(\omega) = \frac{\lambda}{\lambda^2 + \omega^2} \quad [3]$$

and P is the inverse of the data acquisition time. Three resonances were fitted ($N$ = 3), corresponding to the signals from Cho, Cr, and NAA, respectively. This function (Eq. [2]) reflects the experimental lineshape, which was a convolution of a Lorentzian with a sinc function, because the multislice protocol did not allow sufficiently long data acquisition times to record the full NMR signal without truncation.

*In vivo* metabolite concentrations [M] (millimolar) were calculated from:

$$[M] = [P] * \frac{S_0(M)}{S_0(P)} \quad [4]$$

where [P] is the phantom concentration (millimolar) and $S_0$ (M) and $S_0$ (P) are the corrected signals from each voxel of the metabolite and phantom metabolite images, respectively. $S_0$ was calculated as follows: the signals were corrected for (1) $T_1$ and $T_2$ relaxation effects, using Eq. [1], (2) the differential receiver gain used between phantom and human studies, (3) coil loading based on the RF power required to achieve a 90° pulse (see below), and (4) variable degrees of truncation of the NMR signal (because the phantom and metabolites have different $T_2$ relaxation times).

Variable truncation effects were eliminated in the quantitative analysis by applying a variable exponential filter in the time domain (symmetrically around the full-echo signal) so that, after Fourier transformation, all resonances (both *in vivo* and in the phantom) had exactly the same linewidth (i.e., therefore, the same degree of truncation in the time domain).

Loading correction was based on the difference between the RF power required to achieve a 90° pulse (22) in the brain compared with that in the phantom (difference = A, measured in decibels). The corrected signal was calculated, using the relationship

$$S_{corr} = S_{uncorr} * 10^{A/20} \quad [5]$$

An additional check of receiver gain stability and the RF coil loading correction was performed by measurement of the background noise level in the spectroscopic images. A region of noise was measured (100-Hz bandwidth) well downfield from the water resonance, where no signals are expected, but at least 200 Hz away from the edge of the spectrum to avoid possible attenuation effects of the audiofrequency filters. The noise measurement was made in selected voxels outside of the brain, where minimal phase noise would be expected. Minimal variations are expected in the background noise level, provided that the spectrometer has good long-term stability and that inter-subject variations in coil loading are small (22).

To check the accuracy of the correction procedures described above, a set of five phantoms of different ionic strength were prepared; each phantom consisted of 4.6 liters of water, 0.15 to 2.40% by weight being sodium chloride. The water signal, RF noise, and transmitter power required to achieve a 90° pulse were measured in each phantom.

Statistical analysis was performed, using the program "Statview 4.0" (Abacus Concepts Inc, Berkeley, CA). Mean and standard deviation metabolite concentrations were calculated for each brain region. Differences in metabolite levels between different brain regions were examined, using unpaired two-tailed Student's *t*-test. Metabolite levels were also examined for correlation with volunteer age, using linear regression. The level of significance was set at $P < 0.05$.

## RESULTS

All MR images were considered to be normal, with the older subjects showing typical changes such as mild cortical atrophy, ventricular and sulcal widening as expected. None of the volunteers had any white matter hyperintensities on $T_2$ images. Spectroscopic images of the 20 m*M* Cr phantom exhibited uniform image intensity throughout the sample, indicative of good $B_1$ (and $B_0$) field homogeneity. Less than 4% signal variation was noted across the volume of the phantom. In humans, $B_0$ homogeneity was a significant problem in the anterior regions of the most caudal slice, due to the susceptibility effect of the air-tissue interface in the sphenoid sinus. This can be most readily visualized in the field map of Fig. 1B. Phantom Cr $T_1$ and $T_2$ values were 1.12 and 0.61 s, respectively.

Results from the coil loading analysis are shown in Fig. 2. Transmitter power, noise, and signal amplitudes are plotted as a function of the ionic strength of the sample. Fig. 3 shows Cho, NAA, and lactate spectroscopic images from one subject and representative spectra from selected

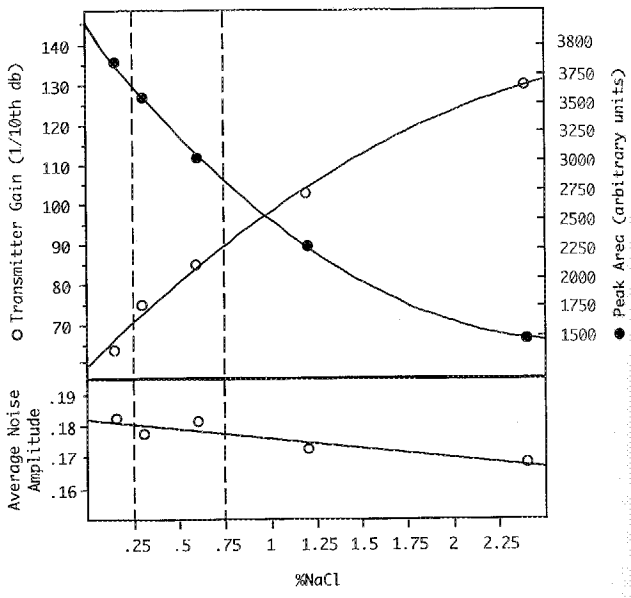


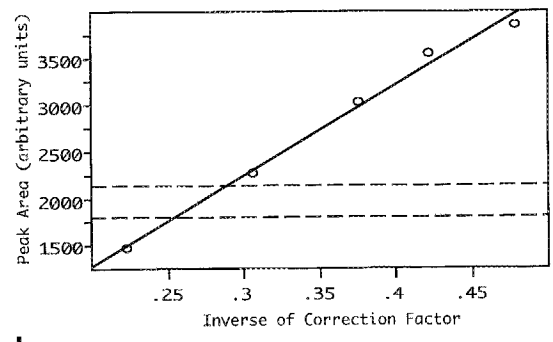


FIG. 2. (A) Transmitter gain required for a 90° pulse, signal amplitude, and average peak-to-peak noise amplitude for five water samples containing different concentrations of sodium chloride. Note the increasing transmitter power and decreased signal amplitude with increased ionic strength. Noise amplitude decreases only slightly. (B) Signal amplitude plotted against the inverse correction factor $10^{A/20}$, showing reasonably good inverse linear correlation. Dashed lines indicate range of typical human RF coil loading conditions.

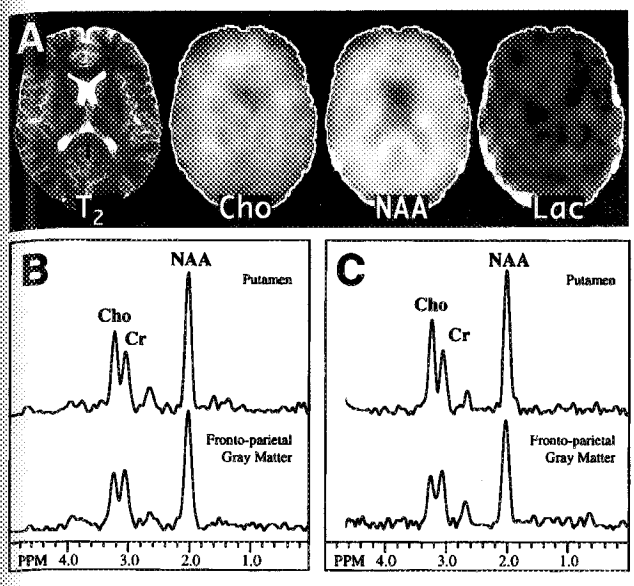


FIG. 3. (A) Spectroscopic images of Cho, Cr, and NAA in a 30-year-old volunteer. Representative spectra from selected regions of interest in a 30-year-old subject (B) and in a 69 year old (C). In particular, notice the increased Cho signals in the putamen of the elderly subject.

regions of interest in a young and an elderly volunteer. Fig. 4 illustrates typical output resulting from the curve-fitting routine.

The results of the quantitative analysis are given in Table 1 and illustrated graphically in Fig. 5. Fig. 6 shows correlation plots for NAA and Cho as a function of age for selected regions of interest, and the corresponding $P$ values are given in Table 2. $P$ values for regional metabolite comparisons are given in Table 3.

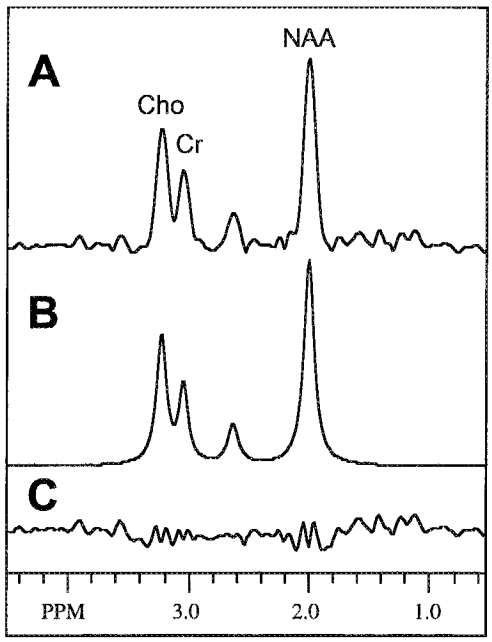


FIG. 4. (A) Representative proton spectrum from the centrum semiovale of one subject. (B) Output from frequency domain curve-fitting routine, using Eq. (2). (C) Residual difference between (A) and (B).

Table 1
Concentrations of Cr, Cho, and NAA in the Normal Human Brain

| | Cho | Cr | NAA |
|---|---|---|---|
| 1. Frontal WM | 2.6 ± 0.7 | 9.5 ± 3.4 | 12.2 ± 3.0 |
| 2. Forceps minor | 2.7 ± 0.6 | 8.9 ± 3.2 | 12.4 ± 3.0 |
| 3. Centrum semiovale | 2.0 ± 0.3 | 6.7 ± 1.4 | 11.3 ± 1.7 |
| 4. Posterior WM | 2.1 ± 0.4 | 7.5 ± 2.0 | 11.2 ± 2.1 |
| 5. Forceps major | 2.4 ± 0.5 | 7.9 ± 2.5 | 13.0 ± 2.7 |
| 6. Genu | 3.2 ± 1.0 | 5.8 ± 3.1 | 13.1 ± 2.5 |
| 7. Splenium | 2.3 ± 0.7 | 6.3 ± 2.6 | 12.3 ± 1.8 |
| 8. Thalamus | 2.5 ± 0.8 | 7.9 ± 2.5 | 10.8 ± 2.8 |
| 9. Putamen | 2.4 ± 0.7 | 9.8 ± 3.7 | 11.2 ± 2.2 |
| 10. Frontoparietal GM | 1.7 ± 0.6 | 8.5 ± 1.6 | 10.3 ± 2.0 |
| "Whole brain average" | 2.4 ± 0.4 | 7.9 ± 1.3 | 11.8 ± 1.0 |

$N$ = 16, mmol, mean ± SD.

## DISCUSSION

### Quantitation Methodology

The phantom replacement method does not require either an internal or external standard but is sensitive to changes in coil loading, receiver gain, and $B_1$ inhomogeneity effects. All of these factors may be accounted for, however. Corrections for coil loading can be applied, based on the 90° pulse power; in the phantom experiments, it was found that a good inverse linear correlation existed between the signal area and the correction factor $10^{A/20}$, (Fig. 2B). Measurements on phantoms indicated that $B_1$ inhomogeneity accounted for less than a 4% variation in SI across the typical volume of a human brain, using the standard GE birdcage head coil, and this factor can generally be ignored for routine studies. Receiver noise levels were found to be virtually constant (<2%) over the range of loading conditions typically encountered in the human head (approximately 2 dB of maximum variation in transmitter gain for a 90° pulse) and, therefore, it is possible to use the background spectral noise level as an independent check of system stability from one scan to the next. Over the much wider range of loading conditions used in the phantom experiments, the receiver noise was found to decrease slightly at higher ionic strengths (Fig. 2A), presumably because of the decreased Q and suboptimal tuning of the RF coil when it is loaded with the most lossy samples.

Inasmuch as all human MR experiments were performed at long-echo times ($TE$ = 272 ms), the largest source of systematic error in the measurements probably arises from errors in the metabolite $T_2$ estimates. Errors will also occur if pathological conditions alter metabolite $T_2$ values, because it is usually impractical to measure metabolite $T_2$s within the time frame of a clinical study. This source of error, however, has to be balanced against the significantly worse water and lipid suppression, as well as interfering resonances from macromolecules, which occur at shorter echo times and which may make definition and measurement of peak areas difficult. In this regard, single-voxel localization methods offer some advantages, because it is usually easier to get good quality short-echo time spectra from single voxels than from spectroscopic images. Short-echo time spectra also exhibit resonances from other compounds, such as glutamine, glutamate and *myo*-inositol, which are not acces-

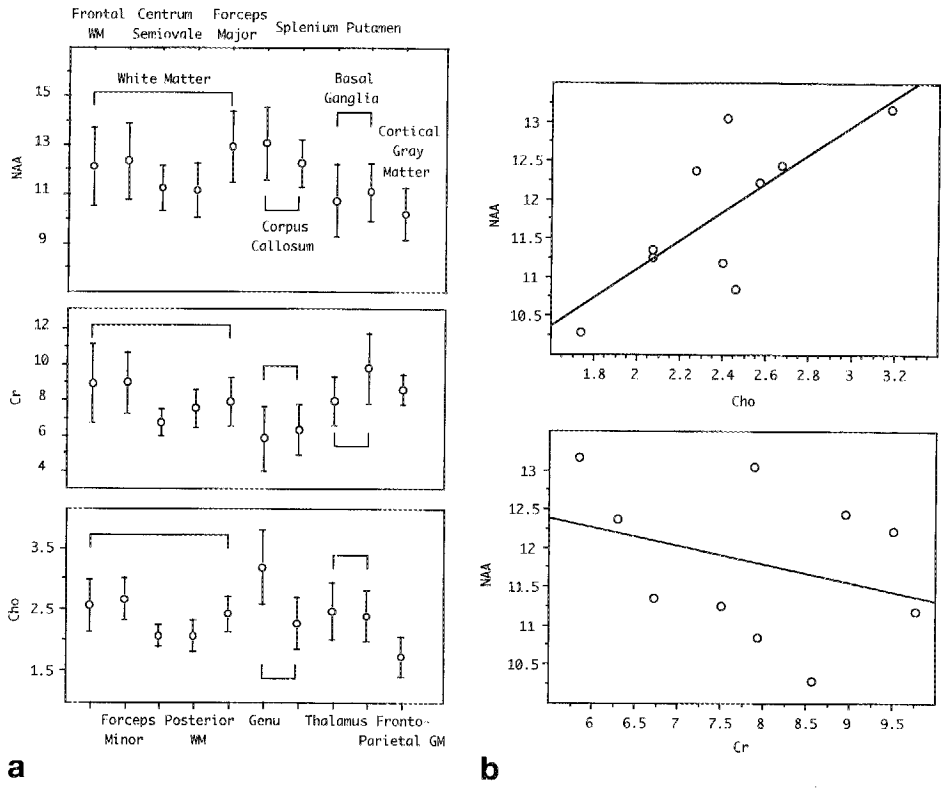


FIG. 5. (A) Plots of NAA, Cr, and Cho (m*M*) as a function of spatial location. Error bars indicate the 95% confidence levels. (B) Correlation plot of NAA versus Cho and NAA versus Cr for all 10 spatial locations. NAA and Cho levels were significantly correlated ($P < 0.02$).

Table 2
Metabolite Variations as a Function of Age: Table of *P* Values from Linear Regression Analysis

| | Cho | Cr | NAA |
|---|---|---|---|
| 1. Frontal WM | **0.0262** | **0.0239** | 0.5188 |
| 2. Forceps minor | 0.4323 | 0.5762 | 0.4357 |
| 3. Centrum semiovale | 0.0712 | 0.4496 | 0.3932 |
| 4. Posterior WM | 0.7332 | 0.9001 | 0.2562 |
| 5. Forceps major | 0.1439 | 0.0536 | 0.6589 |
| 6. Genu | **0.0106** | 0.9992 | 0.9033 |
| 7. Splenium | 0.1298 | 0.4267 | 0.5315 |
| 8. Thalamus | **0.0167** | 0.6519 | 0.5659 |
| 9. Putamen | **0.0124** | 0.8287 | 0.9410 |
| 10. Frontoparietal GM | 0.3514 | 0.9024 | 0.2256 |

Note: Values $P < 0.05$ are printed in boldface type.

sible from long-echo time measurements because of *J*-modulation. Also, although commonly used voxel sizes in single-voxel experiments are usually rather large (e.g., 8 $cm^3$), the edges of the voxel are often better defined, as compared to the rather diffuse point-spread function associated with the spectroscopic imaging data sets.

Another source of error in the multislice data sets may arise from truncation of the NMR signal, because only a relatively short period of time (256 ms, in the current experiments) is available for digitization of the echo. This results in coarse digital resolution in the frequency domain (4 Hz/point, if no zero filling were used). It is, therefore, necessary to zero-fill the data sets several times to ensure adequate digitization of the resonances after Fourier transformation and also to convolute the model lineshape function with the appropriate sinc response. Finally, to avoid errors due to variable amount of truncation, it is important to adjust the digital filter (exponential multiplication) so that the linewidths of the resonances in the *in vivo* spectra match those of the Cr phantom used for the calibration study.

## Metabolite Concentrations

The whole brain metabolite concentration values are in good general agreement with previously determined metabolite values, when one uses single-voxel localization techniques. For instance, a review of 16 studies published between 1988 and 1993 (1) found average metabolite values of 1.7, 7.7, and 11.1 μmol/g of wet weight for Cho, Cr, and NAA, respectively, which is similar to the average values of the current study. These numbers are also in relatively close agreement with recent *in vitro* metabolite concentration measurements in canine brain (1), which showed that the *in vivo* Cho resonance predominantly consists of phosphocholine (0.5 μmol/g) and glycerophosphocholine (GPC, 1.3 μmol/g), and the "Cr" peak consists of Cr (5.9 μmol/g) and phosphocreatine (2.6 μmol/g). A biochemical study of normal elderly human brains (obtained postmortem) also found similar levels of "total" Cho, with less GPC (0.7 μmol/g) and more free Cho (0.3 μmol/g) than in canine brain (23).

## Regional Variations

Although Cr was found to be constant across all locations chosen for analysis, significant regional variations were observed in both Cho and NAA resonances. In agreement with others (20, 24, 25), we found a lower NAA signal in cortical gray matter, as compared to that in most white matter locations, corpus callosum, and basal ganglia. Cho was also significantly lower in cortical gray matter than in white matter. The reasons for these spatial variations are not entirely clear. The reduction of Cho and NAA

Table 3
Regional Metabolite Variations: Table of *P* Values

| | | | | | | | | | |
|---|---|---|---|---|---|---|---|---|---|
| **Cho** | | | | | | | | | |
| FMI | 0.6829 | | | | | | | | |
| CSO | **0.0229** | **0.0019** | | | | | | | |
| PWM | **0.0354** | **0.0046** | | | | | | | |
| FMA | 0.5427 | 0.2397 | **0.0347** | 0.0611 | | | | | |
| GEN | 0.0813 | 0.1113 | **0.0004** | **0.0007** | **0.0171** | | | | |
| SPL | 0.2947 | 0.1221 | 0.3481 | 0.3840 | 0.5325 | **0.0114** | | | |
| TH | 0.7171 | 0.4378 | 0.1009 | 0.1234 | 0.8830 | **0.0492** | 0.5228 | | |
| PT | 0.5398 | 0.2805 | 0.1315 | 0.1616 | 0.9131 | **0.0264** | 0.6547 | 0.8272 | |
| CGM | **0.0024** | **0.0002** | 0.0778 | 0.1120 | **0.0025** | **0.0001** | **0.0437** | **0.0114** | **0.0135** |
| | FWM | FMI | CSO | PWM | FMA | GEN | SPL | TH | PT |
| **Cr** | | | | | | | | | |
| FMI | 0.6441 | | | | | | | | |
| CSO | **0.0060** | **0.0170** | | | | | | | |
| PWM | 0.0569 | 0.1404 | 0.2061 | | | | | | |
| FMA | 0.1444 | 0.3073 | 0.1173 | 0.6446 | | | | | |
| GEN | **0.0059** | **0.0123** | 0.3135 | 0.0866 | 0.0563 | | | | |
| SPL | **0.0070** | **0.0168** | 0.5772 | 0.1552 | 0.0935 | 0.6644 | | | |
| TH | 0.1569 | 0.3291 | 0.1101 | 0.6131 | 0.9641 | 0.0535 | 0.0883 | | |
| PT | 0.8387 | 0.5049 | **0.0042** | **0.0385** | 0.1002 | **0.0040** | **0.0046** | 0.1094 | |
| CGM | 0.3350 | 0.6761 | **0.0017** | 0.1101 | 0.3687 | **0.0047** | **0.0067** | 0.4035 | 0.2387 |
| | FWM | FMI | CSO | PWM | FMA | GEN | SPL | TH | PT |
| **NAA** | | | | | | | | | |
| FMI | 0.8320 | | | | | | | | |
| CSO | 0.3239 | 0.2138 | | | | | | | |
| PWM | 0.2964 | 0.1982 | 0.8807 | | | | | | |
| FMA | 0.4178 | 0.5536 | **0.0425** | **0.0432** | | | | | |
| GEN | 0.3632 | 0.4861 | **0.0285** | **0.0313** | 0.9032 | | | | |
| SPL | 0.8690 | 0.9275 | 0.1172 | 0.1177 | 0.4084 | 0.3261 | | | |
| TH | 0.1880 | 0.1262 | 0.5374 | 0.6415 | **0.0302** | **0.0249** | 0.0774 | | |
| PT | 0.2794 | 0.1877 | 0.8182 | 0.9362 | **0.0424** | **0.0317** | 0.1143 | 0.7006 | |
| CGM | 0.0396 | 0.0221 | 0.1160 | 0.1905 | **0.0025** | **0.0017** | **0.0044** | 0.5208 | 0.2381 |
| | FWM | FMI | CSO | PWM | FMA | GEN | SPL | TH | PT |

Note: Abbreviations as follows: FWM, frontal white matter; FMI, forceps minor; CSO, centrum semiovale; PWM, posterior white matter; FMA, forceps major; GEN, genu of corpus callosum; SPL, splenium of corpus callosum; TH, thalamus; PT, putamen; CGM, cortical gray matter (frontoparietal). Values $P < 0.05$ are printed in boldface type.

may in part be explained by increased CSF content of the region of interest; as can be seen from Fig. 5B, there is a good correlation between Cho and NAA levels in the different spatial locations. However, it should also be noted that Cr levels did not follow the same pattern, with no significant regional variations. Therefore, biochemical changes must play a role, in addition to partial volume effects. No attempt was made in this study to correct for partial volume, and the concentration values listed here are macroscopic millimolar (millimoles per liter of total tissue (parenchyma, CSF, and vascular space)). These values may be divided by the tissue density to convert the measurements to the more common biochemical units micromoles per gram of wet weight. The calculation of true intracellular concentrations requires detailed knowledge of the proportion of the intracellular space within the region of interest and compartmentalization of the metabolite distribution (5, 6), and it was not attempted in the current study.

NAA is often postulated to be solely of neuronal and axonal origin (26) and is known to be absent from mature glial cells (27, 28). Because neuronal density is higher in gray matter than in white matter, the slightly higher NAA concentration in white matter is paradoxical. One possible explanation of this finding is that the NAA $T_2$ is longer in white matter than in gray, although there are conflicting reports as to regional variations in metabolite $T_2$s in the literature (24, 29). Another possibility is that the larger white matter signal is due to increased contributions of *N*-acetyl-aspartyl-glutamate, which is present in higher concentrations in white matter than in gray matter (7, 30).

The reasons for the higher Cho concentration in white matter is also unclear. Although myelin contains phosphatidylcholine at very high concentrations (20 m*M* (31)), this compound is almost certainly not NMR visible (particularly at long-echo times) because of its low mobility. However, because the Cho resonance predominantly consists of phosphocholine and GPC (1), compounds that are involved in membrane synthesis and degradation, the higher Cho in white matter may reflect the increased demand for myelin membrane synthesis in white matter, as compared to that in gray matter.

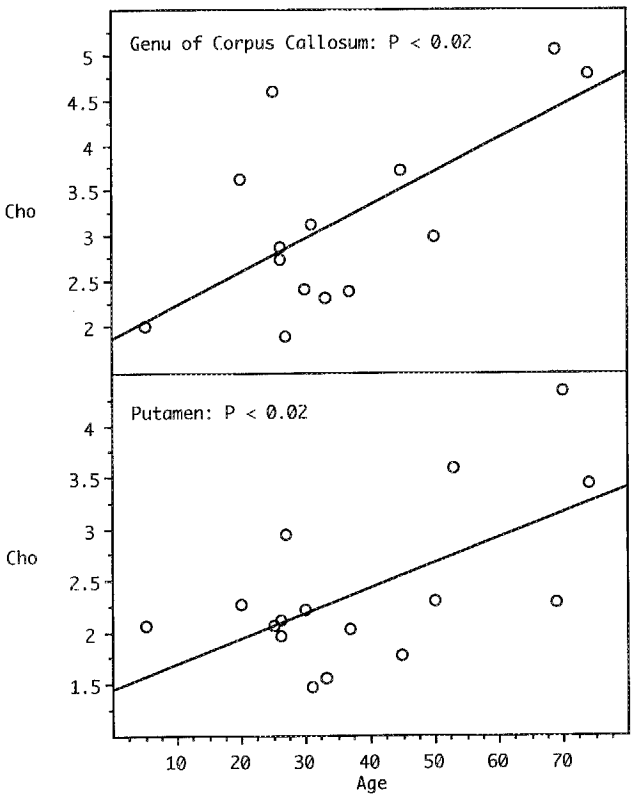


FIG. 6 Regression plots of (A) Cho (m*M*) and (B) NAA (m*M*) as a function of age in selected regions of the brain. Cho was found to significantly ($P < 0.02$) increase with age in the genu of the corpus callosum, putamen, thalamus (not shown), and frontal white matter (not shown). No significant age-related changes were observed in NAA, although some voxels did show a trend toward decreasing NAA with increasing age.

### Age Variations

Metabolite levels were also examined in each brain location for age-related variations. No significant changes were found in NAA or Cr as a function of age in the current study population, with the exception of an increase in Cr in frontal white matter (Table 2). However, Cho was found to significantly increase with age in thalamus, putamen, genu of the corpus callosum, and frontal white matter.

Although it has been a generally accepted dogma that neuronal density gradually decreases with age (32), more recently, this view has been challenged (33). Terry *et al.* (33) found that although brain mass significantly decreased with age, total neocortical neuronal density did not change. Instead, there was a relative decline in large neuron counts, which was offset by an increase in the number of small neurons. There was also a significant increase in glial cells. The current MR data is concordant with the hypothesis that total neuronal density does not change with age, inasmuch as no significant changes in NAA were observed in any brain region. However, it has also been pointed that there may be large interindividual variations in neuronal density (34, 35), and that statistically significant results may only be obtained in large study groups. Therefore, further studies, with a greater number of elderly subjects, may yet reveal significant changes in NAA levels in the aging brain.

The increase in the Cho signal, which was observed in several different locations in both gray and white matter, presumably reflects the increasing number of glial cells (33) that are reported to have high Cho signals (27, 28). It is particularly important to recognize this effect, because elevated Cho is commonly observed in many pathological conditions (36–40); in the absence of an age-matched control subject, high Cho signals in elderly individuals could erroneously be considered to be abnormal.

In summary, the phantom replacement method is a rapid and convenient means of quantitating multislice spectroscopic imaging data sets. The method is robust, with only small interindividual variations, and does not require any additional scans to be performed. Provided that care is taken to use the appropriate correction factors, accurate concentration values can be obtained, which are in good agreement with previous values determined using single-voxel localization techniques.

## ACKNOWLEDGMENTS

The spectroscopic imaging pulse sequence was developed at the NIH *in vivo* NMR Center in Bethesda, MD by Dr. Chrit Moonen and his colleagues.

## REFERENCES

1. P. Barker, S. Breiter, B. Soher, J. Chatham, J. Forder, M. Samphilipo, C. Magee, J. Anderson, Quantitative proton spectroscopy of canine brain: *in vivo* and *in vitro* correlations. *Magn. Reson. Med.* **32**, 157–163 (1994).
2. J. Hennig, H. Pfister, T. Ernst, D. Ott, Direct absolute quantification of metabolites in the human brain with *in vivo* localized proton spectroscopy. *NMR Biomed.* **5**, 193–199 (1992).
3. P. B. Barker, B. J. Soher, S. J. Blackband, J. C. Chatham, V. P. Mathews, R. N. Bryan, Quantitation of proton NMR spectra of the human brain using tissue water as an internal concentration reference. *NMR Biomed.* **6**, 89–94 (1993).
4. P. Christiansen, O. Henriksen, M. Stubgaard, P. Gideon, H. Larsson, In vivo quantification of brain metabolites by 1H-MRS using water as an internal standard. *Magn. Reson. Imaging* **11**, 107–118 (1993).
5. T. Ernst, R. Kreis, B. Ross, Absolute quantitation of water and metabolites in the human brain. I. Compartments and

water. *J. Magn. Reson. B.* **102,** 1–8 (1993).
6. R. Kreis, T. Ernst, B. Ross, Absolute quantitation of water and metabolites in the human brain. II. Metabolite concentrations. *J. Magn. Reson. B.* **102,** 9–19 (1993).
7. T. Michaelis, K.-D. Merboldt, H. Bruhn, W. Hanicke, J. Frahm, Absolute concentrations of metabolites in the adult human brain *in vivo*: quantification of localized proton MR spectra. *Radiology* **187,** 219–227 (1993).
8. O. A. C. Petroff, D. D. Spencer, J. R. Alger, J. W. Prichard, High-field proton magnetic resonance spectroscopy of human cerebrum obtained during surgery for epilepsy. *Neurology* **39,** 1197–1202 (1989).
9. T. Brown, B. Kincaid, K. Uğurbil, NMR Chemical shift imaging in three dimensions. *Proc. Natl. Acad. Sci. (USA)* **79,** 3523–3526 (1982).
10. A. A. Maudsley, D. B. Twieg, M. D. Sappey, B. Hubesch, J. W. Hugg, G. B. Matson, M. W. Weiner, Spin echo 31P spectroscopic imaging in the human brain. *Magn. Reson. Med.* **14,** 415–422 (1990).
11. J. Duyn, J. Gillen, G. Sobering, P. van Zijl, C. Moonen, Multislice proton MR spectroscopic imaging of the brain. *Radiology* **188,** 277–282 (1993).
12. D. M. Spielman, J. M. Pauly, A. Macovski, G. H. Glover, D. R. Enzmann, Lipid-suppressed single- and multisection proton spectroscopic imaging of the human brain. *J. Magn. Reson. Imaging* **2,** 253–262 (1992).
13. J. R. Alger, S. C. Symko, A. Bizzi, S. Posse, D. J. DesPres, M. R. Armstrong, Absolute quantitation of short TE brain 1H-MR spectra and spectroscopic imaging data. *J. Comput. Assist. Tomogr.* **17,** 191–199 (1993).
14. C. Husted, J. Duijn, G. Matson, A. Maudsley, M. Weiner, Molar quantitation of in vivo proton metabolites in human brain with 3D MR spectroscopic imaging. *Magn. Reson. Imaging* **12,** 661–667, (1994).
15. C. T. Moonen, P. C. M. van Zijl, J. Gillen, P. Daly, M. von Kienlin, J. Wolf, J. Cohen, Comparison of single-shot localization methods (STEAM and PRESS) for *in vivo* proton NMR spectroscopy. *NMR Biomed.* **2,** 201–208 (1989).
16. P. S. Tofts, S. Wray, A critical assessment of methods of measuring absolute metabolite concentrations by NMR spectroscopy. *NMR Biomed.* **1,** 1–10 (1988).
17. A. Haase, J. Frahm, W. Hanicke, D. Matthei $^1$H NMR chemical shift selective imaging. *Phys. Med. Biol.* **30,** 341–344 (1985).
18. C. T. W. Moonen, P. C. M. van Zijl, Highly effective water suppression for *in vivo* proton NMR spectroscopy (DRYSTEAM). *J. Magn. Reson.* **88,** 28–41 (1990).
19. D. Marion, M. Ikura, A. Bax, Improved solvent suppression in one- and two-dimensional NMR spectra by convolution of time-domain data. *J. Magn. Reson.* **84,** 425–430 (1989).
20. G. Tedeschi, A. Bertolino, A. Righini, G. Campbell, R. Raman, J. H. Duyn, C. T. W. Moonen, J. H. Alger, G. Di Chiro, Brain regional distribution pattern of metabolite signal intensities in young adults by proton magnetic resonance spectroscopic imaging. *Neurology* **45,** 1384–1391 (1995).
21. W. H. Press, B. P. Flannery, S. A. Teukolsky, W. T. Vetterling, Minimization or maximization of function, *in* "Numerical Recipes in C: The Art of Scientific Computing," pp. 290–352, Cambridge University Press, Cambridge, UK, 1988.
22. D. I. Hoult, R. E. Richards, The signal-to-noise ratio of the nuclear magnetic resonance experiment. *J. Magn. Reson.* **24,** 71–85 (1976).
23. R. M. Nitsch, J. K. Blusztajn, A. G. Pittas, B. E. Slack, J. H. Growdon, R. J. Wurtman, Evidence for a membrane defect in Alzheimer disease brain. *Proc. Natl. Acad. Sci.* (USA) **89,** 1671–1675 (1992).
24. H. P. Hetherington, G. F. Mason, J. W. Pan, S. L. Ponder, J. T. Vaughan, D. B. Tweig, G. M. Pohost, Evaluation of cerebral gray and white matter metabolite differences by spectroscopic imaging at 4.1T. *Magn. Reson. Med.* **32,** 565–571 (1994).
25. G. Tedeschi, A. Righnin, A. Bizzi, A. S. Barnett, J. R. Alger, Cerebral white matter in the centrum semiovale exhibits a larger N-acetyl signal than does gray matter in long echo time 1H-magnetic resonance spectroscopic imaging. *Magn. Reson. Med.* **33,** 127–133 (1995).
26. D. L. Birken, W. H. Oldendorf, N-acetyl-L-aspartic acid: a literature review of a compound prominent in $^1$H-NMR spectroscopic studies of brain. *Neurosci. Biobehav. Rev.* **13,** 23–31 (1989).
27. S. S. Gill, R. K. Small, D. G. Thomas, P. Patel, R. Porteous, N. van Bruggen, D. G. Gadian, R. A. Kauppinen, S. R. Williams, Brain metabolites as 1H NMR markers of neuronal and glial disorders. *NMR Biomed.* **2,** 196–200 (1989).
28. S. S. Gill, D. G. Thomas, B. N. Van, D. G. Gadian, C. J. Peden, J. D. Bell, I. J. Cox, D. K. Menon, R. A. Iles, D. J. Bryant, Proton MR spectroscopy of intracranial tumours: in vivo and in vitro studies. *J. Comput. Assist. Tomogr.* **14,** 497–504 (1990).
29. J. Frahm, H. Bruhn, M. L. Gyngell, K. D. Merboldt, W. Hanicke, R. Sauter, Localized proton NMR spectroscopy in different regions of the human brain *in vivo*. Relaxation times and concentrations of cerebral metabolites. *Magn. Reson. Med.* **11,** 47–63 (1989).
30. J. Frahm, T. Michaelis, K.-D. Merboldt, W. Hanicke, M. L. Gyngell, H. Bruhn, On the N-acetyl methyl resonance in localized $^1$H NMR spectra of the human brain *in vivo*. *NMR Biomed.* **4,** 201–204 (1991).
31. B. L. Miller, A review of chemical issues in $^1$H NMR spectroscopy: *N*-acetyl-L-aspartate, creatine and choline. *NMR Biomed.* **4,** 47–53 (1991).
32. G. Henderson, B. E. Tomlinson, P. H. Gibson, Cell counts in human cerebral cortex in normal adults throughout life using an image analysis computer. *J. Neurol. Sci.* **46,** 113–136 (1980).
33. R. D. Terry, R. DeTeresa, L. A. Hansen, Neocortical cell counts in normal human adult aging. *Ann. Neurol.* **21,** 530–539 (1987).
34. R. D. Terry, Some biological aspects of the aging brain. *Mech. Ageing Dev.* **14,** 191–201 (1980).
35. R. Katzman, R. Terry, *in* "The Neurology of Aging" (F. Plum, J. R. Baringer, S. Gilman, Eds.), p. 249, F.A. Davis, Philadelphia, 1983.
36. P. B. Barker, R. R. Lee, J. C. McArthur, AIDS dementia complex: evaluation with proton MR spectroscopic imaging. *Radiology* **195,** 58–64 (1995).
37. P. B. Barker, J. H. Gillard, P. C. M. van Zijl, B. J. Soher, D. F. Hanley, A. M. Agildere, S. M. Oppenheimer, R. N. Bryan, Acute stroke: evaluation with serial proton MR spectroscopic imaging. *Radiology* **192,** 723–732 (1994).
38. B. Kruse, P. B. Barker, P. C. M. van Zijl, J. H. Duyn, C. T. W. Moonen, H. W. Moser, Multislice proton MR spectroscopic imaging in X-linked adrenoleukodystrophy. *Ann. Neurol.* **36,** 595–608 (1994).
39. C. A. Davie, C. P. Hawkins, G. J. Barker, A. Brennan, P. S. Tofts, D. H. Miller, W. I. McDonald, Detection of myelin breakdown products by proton magnetic resonance spectroscopy [letter]. *Lancet* **341,** 630–631 (1993).
40. J. R. Alger, J. A. Frank, A. Bizzi, M. J. Fulham, B. X. DeSouza, M. O. Guhaney, S. W. Inscoe, J. L. Black, P. C. M. van Zijl, C. T. W. Moonen, G. Di Chiro, Metabolism of human gliomas: assessment with H-1 MR spectroscopy and F-18 fluorodeoxyglucose PET. *Radiology* **177,** 633–641 (1990).